

Local $\pm[001]_c$ off-centering nanoregions in silver niobate

Cite as: J. Appl. Phys. **131**, 124107 (2022); <https://doi.org/10.1063/5.0084467>

Submitted: 06 January 2022 • Accepted: 12 March 2022 • Published Online: 30 March 2022

 Gen Li,  Hai Liu,  Lei Zhao, et al.



View Online



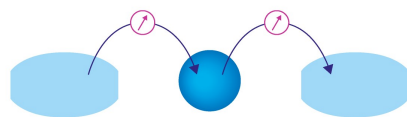
Export Citation



CrossMark

Webinar

Interfaces: how they make
or break a nanodevice



March 29th – Register now

 Zurich
Instruments

Local $\pm[001]_c$ off-centering nanoregions in silver niobate

Cite as: J. Appl. Phys. 131, 124107 (2022); doi: 10.1063/5.0084467

Submitted: 6 January 2022 · Accepted: 12 March 2022 ·

Published Online: 30 March 2022



View Online



Export Citation



CrossMark

Gen Li,^{1,2,3,a)} Hai Liu,¹ Lei Zhao,⁴ Jing Gao,⁴ Jing-Feng Li,⁴ and Jing Zhu^{1,3,a)}

AFFILIATIONS

¹National Center for Electron Microscopy in Beijing, School of Materials Science and Engineering, The State Key Laboratory of New Ceramics and Fine Processing, Key Laboratory of Advanced Materials (MOE), Tsinghua University, Beijing 100084, People's Republic of China

²Department of Conservation Science and Technology, The Palace Museum, Beijing 100009, People's Republic of China

³Ji Hua Laboratory, Foshan, Guangdong Province 528000, People's Republic of China

⁴School of Materials Science and Engineering, The State Key Laboratory of New Ceramics and Fine Processing, Tsinghua University, Beijing 100084, People's Republic of China

a)Authors to whom correspondence should be addressed: g-li14@tsinghua.org.cn. Tel.: +86 010-85007294 and jzhu@mail.tsinghua.edu.cn. Tel.: +86 010-62794026

ABSTRACT

As a typical lead-free antiferroelectric material, silver niobate has attracted much attention in recent years due to its excellent performance in energy storage. In this work, based on a spherical aberration-corrected STEM-high angle annular dark field technique, the sites of each cation column of pure silver niobate and Ta-doped silver niobate were quantitatively obtained. Besides conventional antiferroelectric displacements along the $\pm[1-10]_c$ directions, B-site ions were found to also deviate along $\pm[001]_c$ directions and form many local off-centering nanoregions, which may induce weak ferroelectricity, just like polar nanoregions in relaxed ferroelectrics. Such results will further increase our understanding of silver niobate in the microscopic view and may help explain some unsolved questions.

Published under an exclusive license by AIP Publishing. <https://doi.org/10.1063/5.0084467>

I. INTRODUCTION

Antiferroelectric material is an important class of functional material. They can be used in antiferroelectric-ferromagnetic heterojunctions^{1–6} and in actuators in microelectromechanical systems^{7,8} and applied as piezoelectric material.⁹ Nevertheless, they are more widely used in electrostatic energy storage devices. The most widely studied antiferroelectric energy storage materials are lead zirconate¹⁰ and its doped products.^{11–17} Today's researchers are more eager to realize high energy storage density in environmentally friendly lead-free systems, such as $\text{Na}_{0.5}\text{Bi}_{0.5}\text{TiO}_3\text{-Sr}_{0.7}\text{Bi}_{0.2}\text{TiO}_3$ multilayer ceramic¹⁸ and $\text{BiFeO}_3\text{-BaTiO}_3\text{-SrTiO}_3$ dielectric films,¹⁹ but they belong to dielectric energy storage systems. When it comes to antiferroelectric energy storage materials, silver niobate is still one candidate with high expectations.

Silver niobate has a perovskite structure, and its lattice constant along the $\pm[001]_c$ directions is four times the original one due to the antiferroelectric displacements of cations along $\pm[110]_c$

directions.²⁰ After first being synthesized in the 1950s,²¹ researchers mainly focused on its structure and phase transitions^{22–31} and tried to analyze it with first-principles calculations.^{32–35} In summary, antiferroelectric phase Pbcm and ferrielectric phase Pmc_2l exist simultaneously below 340 K; between 340 and 626 K, there is only phase Pbcm , and as temperature rises above 626 K, several paraelectric phases appear in turn: orthorhombic phase Cmcm , tetragonal phase $\text{P}4/\text{mbm}$, and cubic phase $\text{Pm}\bar{3}\text{m}$, to name a few.

The study of silver niobate as a functional material possibly dates back to 2007, when Fu *et al.* found a polarization up to $52 \mu\text{C}/\text{cm}^2$ and double hysteresis P-E loop in a silver niobate polycrystal.²⁸ In 2016, Tian *et al.* realized an energy storage density of $2.1 \text{ J}/\text{cm}^3$ in pure silver niobate.³⁶ When doped with only one of the following elements, Mn, W, Bi, Ta, La, Sm, and Gd, the corresponding energy storage density could achieve 2.5, 3.0, 3.3, 4.2, 4.4, 4.5, and $4.5 \text{ J}/\text{cm}^3$.^{37–43} Using two doping elements in both the A-site and B-site could further enhance the

energy storage property; the corresponding value was 4.6 J/cm^3 when doped with Bi and Zn,⁴⁴ 4.87 J/cm^3 when doped with Sm and Ta,⁴⁵ and 6.5 J/cm^3 when doped with Nd and Ta.⁴⁶ Besides doping, the energy storage behavior was also found to correlate with the existing form of materials. The energy storage density of pure silver niobate was 2.59 J/cm^3 after a better sintering process,⁴⁷ and could even increase to 5.8 J/cm^3 when it took the form of a thin film grown by PLD.⁴⁸

However, despite the rapid enhancement of energy storage density, a knowledge of antiferroelectric materials, such as silver niobate, at the atomic scale is still far from enough. For example, based on an analysis of diffuse scattering lines in the diffraction patterns of silver niobate, Levin *et al.* previously speculated that B-site niobium ions possess not only periodic antiferroelectric displacements along the $\pm[1-10]_c$ directions, which has been confirmed in our previous work,^{49,50} but also correlated $\pm[001]_c$ displacements in the microscopic view.³⁰ Since the macroscopic structure of silver niobate is the random mixture of these local displacement structures, B-site niobium ions did not exhibit displacement along the $[001]_c$ direction in macroscopic measurements,³⁰ but it was not directly proved due to the restriction of electron microscopy at that time. The absence of atomic-scale information limits our understanding of antiferroelectric materials, especially the relationship between their physical properties and microstructures.

Fortunately, the development of modern microscopy makes it possible for us to observe the atomic-scale structures of antiferroelectrics, and many new properties have been revealed. For instance, traditional antiferroelectric material PbZrO_3 will manifest incommensurate modulations or ferrielectric characteristics after chemically modified to be the $(\text{Pb}, \text{Nb})(\text{Zr}, \text{Sn}, \text{Ti})\text{O}_3$ system⁵¹ and $(\text{Pb}, \text{La})(\text{Zr}, \text{Sn}, \text{Ti})\text{O}_3$ system,⁵² which can be directly observed with the STEM technique. In this work, based on atomic-scale resolution images of silver niobate and Ta-doped silver niobate, the lateral $\pm[001]_c$ off-centering distribution of B-site niobium ions was further analyzed. The sites of cation columns in the STEM-High Angle Annular Dark Field (HAADF) images of silver niobate and Ta-doped silver niobate were quantitatively obtained with the peak finding and Gaussian fitting techniques. Our analysis results are basically consistent with those predicted by Levin *et al.* and revealed more details. Such results may further enhance our understanding of antiferroelectric materials such as silver niobate in the microscopic view, for instance, explaining the remnant polarization problem of silver niobate and its doping derivates.

II. EXPERIMENTAL

AgNbO_3 ceramics were prepared by the conventional solid-state reaction method using Ag_2O ($\geq 99.7\%$) and Nb_2O_5 ($\geq 99.99\%$) powders as the raw materials. These oxide powders were mixed using a planetary ball mill with anhydrous ethanol at 250 rpm for 24 h in a nylon jar with zirconia ball media. The dried powder mixture was pressed into disks of 20 mm in diameter and 2 mm in thickness and calcined at 900°C for 6 h in an O_2 atmosphere. The calcined powders were milled again and pressed into disks of 8 mm in diameter and 1.2 mm in thickness, followed by cold isostatic pressing under 220 MPa for 1.5 min. After that, the samples were

sintered at 1100°C for 6 h in the O_2 atmosphere to prevent the possible decomposition of the silver oxide at high temperature.

Selected area electron diffraction patterns were acquired using JEOL 2010F TEM with a double tilting stage, operating at 200 kV. High Resolution Scanning Transmission Electron Microscope (HRSTEM) experiments were performed using a spherical-aberration-corrected Titan Themis TEM with a double tilting stage, operating at 300 kV, and the STEM detector was a High Angle Annular Dark Field (HAADF) detector, with a camera length of 115 mm, and the corresponding collection semi-angle range was 48–200 mrad. The samples for TEM experiments were first mechanically polished to $30 \mu\text{m}$. After that, a pit meter was used to grind a curved pit on the sample surface. The thickness of the pit bottom was about $10 \mu\text{m}$. Then, the samples were ion-milled to reach electron transparency with the BAL-TEC RES101 system, in which Ar-ion beams operated at 0.1–4 kV. All the image filtering, peak finding, Gaussian fitting, and statistical work were performed with the self-made MATLAB code.

III. RESULTS AND DISCUSSION

Figures 1(a)–1(d) are diffraction patterns of silver niobate under four zone axes $[130]_c$, $[03-1]_c$, $[120]_c$, and $[02-1]_c$, respectively. It should be noted that although we use the pseudo-cubic coordinates in this paper, the several $\langle 001 \rangle_c$ and $\langle 110 \rangle_c$ directions of AgNbO_3 are not equivalent, because the antiferroelectric dipoles

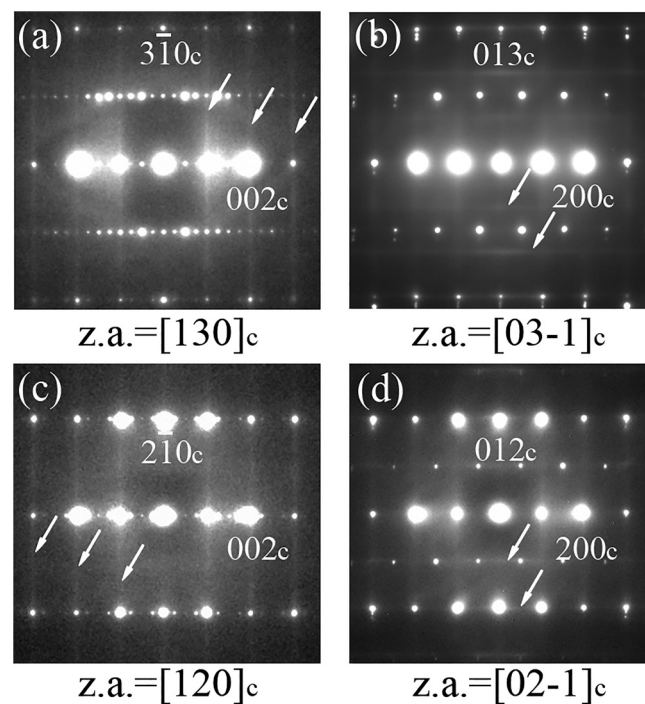


FIG. 1. (a)–(d) are diffraction patterns of silver niobate under $[130]_c$, $[03-1]_c$, $[120]_c$, and $[02-1]_c$ zone axes, respectively, in which the diffuse scattering lines are pointed out by arrows.

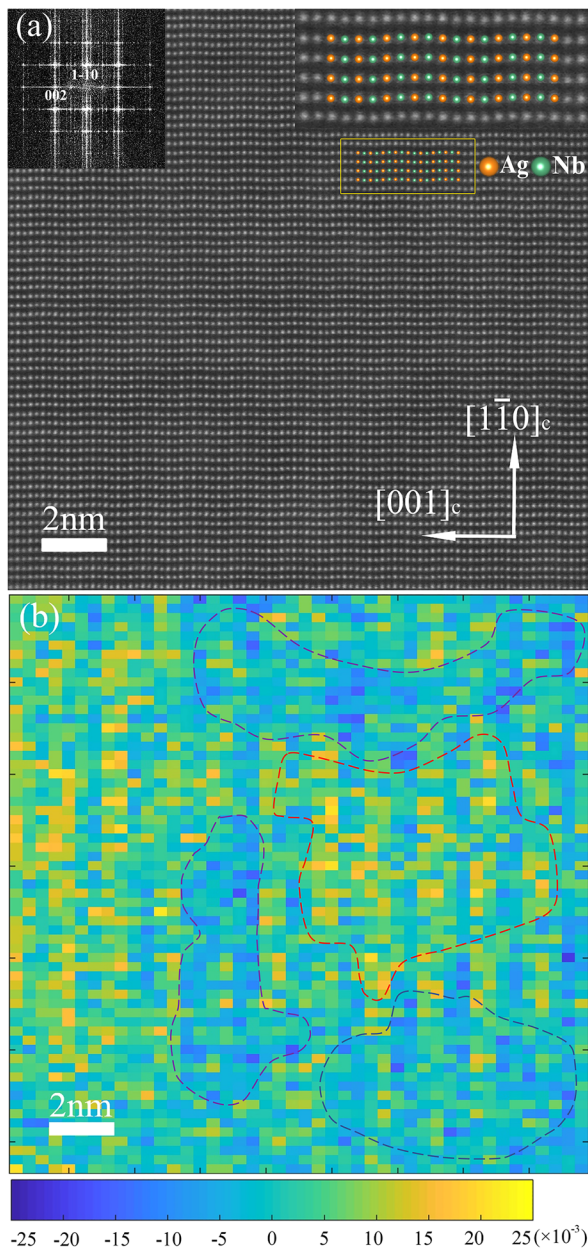


FIG. 2. (a) HAADF image of silver niobate, in which the upper-right illustration is the enlarged view of the orange rectangular area. The orange spots and green spots stand for silver atoms and niobium atoms, respectively. The upper-left illustration is its Fourier transform. (b) $\pm[001]_c$ off-centering mapping of B-site niobate atoms.

define a special direction or zone axis in the crystal lattice. In this paper, we define the special zone axis under which antiferroelectric displacements can be observed to be $[110]_c$; therefore, the antiferroelectric displacements exist in the $\pm[1-10]_c$ directions.

Diffuse scattering lines, which are indicated by white arrows in each figure, are consistent with previous results reported by Levin *et al.*³⁰ All the diffuse scattering lines (indicated by white arrows) in Figs. 1(a) and 1(c) are perpendicular to the reciprocal $[001]_c$ vector and parallel with reciprocal $[3-10]_c$ and $[2-10]_c$ vectors, while the diffuse scattering lines in Figs. 1(b) and 1(d) are perpendicular to the reciprocal $[013]_c$ and $[012]_c$ vectors and parallel with reciprocal $[200]_c$ vector.

According to Fig. 1, it will not be difficult to find that the diffuse lines are the intersecting lines between the $[001]_c$ diffuse sheets [or $(001)_c$ reciprocal planes] and the corresponding diffraction planes, because the diffraction planes are also planes in the reciprocal space, and all they reflect is the presence of one-dimensional correlations along the $[001]_c$ direction. On the other hand, no such clear diffuse scattering lines are observed perpendicular to two other cubic directions (i.e., $[100]_c$ and $[010]_c$). Therefore, the possible correlated Nb displacements exist only in the $[001]_c$ directions under room temperature. In order to further study the correlated displacements along the $[001]_c$ direction, the most effective method is to directly observe the atomic structure with a modern electron microscope.

Figure 2(a) is the STEM-HAADF image of silver niobate. The quantitative position coordinates of each atom can be acquired after peak finding and Gaussian fitting, and then, the atomic displacement along the $\pm[001]_c$ directions can be calculated. In our experiments, the STEM fast scanning direction was parallel to the $[001]_c$ direction, which is also parallel to the direction of the atomic arrangement A-B-A. When measuring the displacement of the B-site atom relative to its two neighboring A-site atoms, such a setting can minimize the error caused by the drifting effect to the greatest extent and improve the accuracy of analysis.⁵³ Owing to the fact that the Ag atoms may also display order-disorder behavior similar to that of Nb atoms,⁵⁴ it would be more proper to use “off-centering” than “displacement” in this situation, and one parameter ζ is defined to express it.

First, one analysis unit is defined as three consecutive Ag-Nb-Ag atoms arranged along the $[001]_c$ direction; hence, each analysis unit contains only one B-site niobium atom. If the coordinates of these three atoms in the $[001]_c$ direction are denoted as x_{A1} , x_B , and x_{A2} from left to right, then parameter ζ is defined as

$$\zeta = \frac{x_B - x_{A1}}{x_{A2} - x_{A1}} - \frac{1}{2}. \quad (1)$$

Relative to the center of the analysis unit, namely, the midpoint of two A-site atoms in the left and the right sides, the B-site niobium atom moves to the right when $\zeta > 0$ and to the left when $\zeta < 0$. After peak finding and Gaussian fitting, the off-centering parameter ζ of each niobium atom can be calculated from the HAADF image and the corresponding $\pm[001]_c$ off-centering distribution mapping can be drawn, as shown in Fig. 2(b).

As shown in Fig. 2(b), B-site niobium atoms in three regions surrounded by purple dashed lines move to the left, in the neighboring region surrounded by a red dashed line, niobium atoms move to the right, while in the interfaces between these regions, the displacements are quite small. Such a localized ordered off-centering behavior is quite similar to that in the polar nanoregion

in relaxed ferroelectric materials, and, therefore, it can be named as the $\pm[001]_c$ off-centering nanoregion. If the diameter of the nanoregion is roughly defined as the largest distance between two points in it, then the diameters of these four displacement nanoregions are on the order of 10 nm.

At first glance, the off-centering behavior of the niobium atoms shown in Figs. 2(a) and 2(b) seems to be different from the speculation of diffuse lines, which implies the presence of one-dimensional correlations along the $[001]_c$ direction. However, these correlated displacements can be dynamic or static in nature (or a mix), and we cannot separate these two effects from diffraction patterns. What STEM imaging reveals is the static nature of the domains, which may differ from the result given by diffraction that reflects an instantaneous structure.

In order to prove that the $\pm[001]_c$ off-centering nanoregion observed is universal, HAADF images from different sample areas were further acquired and processed with the identical method, as shown in Fig. 3, where the white scale bar is 2 nm. All the original STEM-HAADF images, and the corresponding off-centering domain figures, were taken under the zone axis $[110]_c$, and all the displacement domains shown in Fig. 3 present displacements only along the $\pm[001]_c$ directions but not along either $[100]_c$ or $[010]_c$.

As seen in Fig. 3, all these sub-figures contain lateral $\pm[001]_c$ off-centering nanoregions similar to those in Fig. 2(b), but such nanoregions do not have a regular shape or a specific orientation. Almost exactly the same processes were applied to Ta-doped silver niobate, and Fig. 4 shows the results.

As shown in Figs. 3 and 4, the $\pm[001]_c$ off-centering distributions in silver niobate and Ta-doped silver niobate are similar but not identical. The $\pm[001]_c$ off-centering nanoregions exist in both pure silver niobate and Ta-doped silver niobate. From the first glimpse, the off-centering value and the nanoregion size of pure silver niobate are larger than those of Ta-doped silver niobate. However, the shapes of the off-centering nanoregions are irregular, which makes it difficult to compare the results of these two samples. In order to further characterize the $\pm[001]_c$ off-centering distributions in both systems, two parameters based on statistics can be introduced,

$$\begin{cases} D1 = \frac{1}{N} \sum_{i=1}^N |\zeta_i|, \\ D2 = \frac{1}{N} \sum_{i=1}^N \zeta_i, \end{cases}$$

where ζ_i is the $\pm[001]_c$ off-centering of the i th B-site atom in each image and N is the number of niobate atoms in each image. $D1$ is the averaged absolute value of each $\pm[001]_c$ off-centering, and $D2$ is the averaged net value of each $\pm[001]_c$ off-centering. Generally speaking, $D1$ is related to the maximum off-centering value in each $\pm[001]_c$ off-centering region, while $D2$ is related to the region size when the field of view is fixed: if there are many independent $\pm[001]_c$ off-centering regions in one field of view, the off-centering values of B-site atoms will cancel out and the averaged net value $D2$ will be close to zero; but if the number of $\pm[001]_c$ off-centering regions in a specific field of view is small, the averaged net value of $\pm[001]_c$ off-centering of B-site atoms will not be canceled out, and may be even close to $D1$

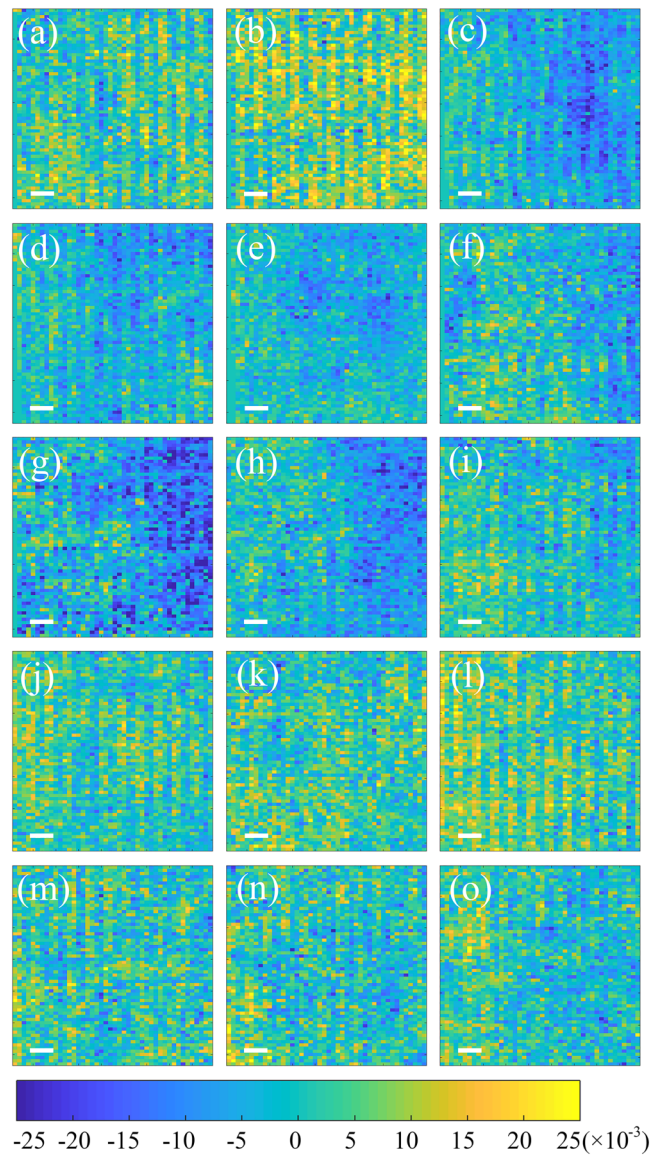


FIG. 3. (a)–(o) Calculated $\pm[001]_c$ off-centering mapping results of B-site niobate atoms in silver niobate of 15 different image areas. The scale bar is 2 nm. The orange and blue colors stand for displacements of B-site niobate atoms along the $-[001]_c$ direction (right direction) and the $+[001]_c$ direction (left direction), respectively.

under the extreme condition that the $\pm[001]_c$ off-centering region size is close to or larger than the field of view.

Figure 5 shows the averaged $\pm[001]_c$ off-centering of silver niobate and Ta-doped silver niobate. The horizontal coordinate is the $D1$ value of each image, and the vertical coordinate is the $D2$ value of each image. It can be seen that both the $D1$ values and $D2$ values of pure silver niobate are larger than those of Ta-doped silver

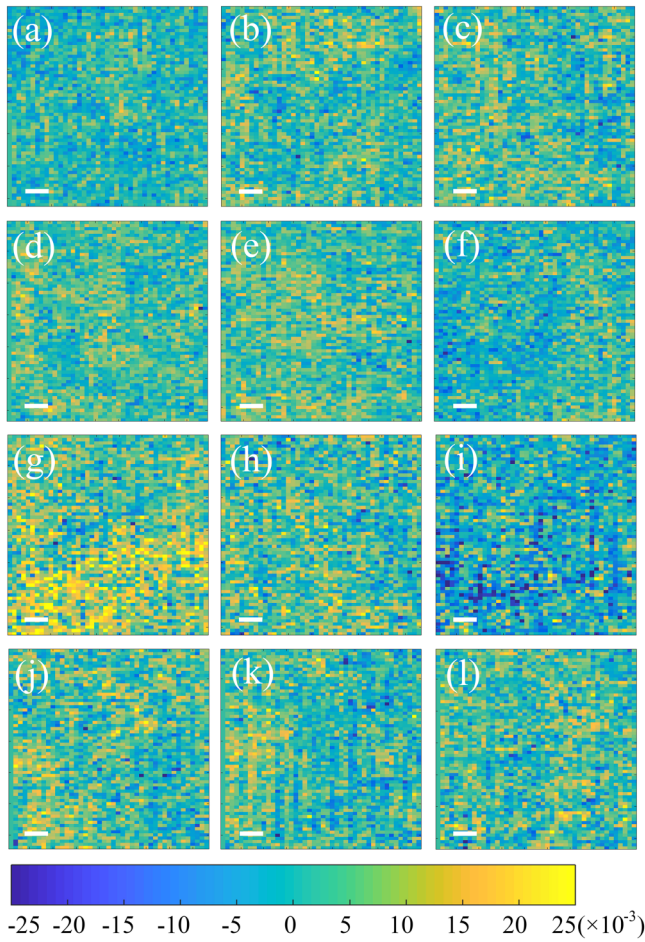


FIG. 4. (a)–(l) Calculated $\pm[001]_c$ off-centering mapping results of B-site niobate atoms in Ta-doped silver niobate of 12 different image areas. The scale bar is 2 nm. The orange and blue colors stand for displacements of B-site niobate atoms along the $-[001]_c$ direction (right direction) and the $+[001]_c$ direction (left direction), respectively.

niobate. Based on the discussion above, it can be inferred that the $\pm[001]_c$ off-centering regions of Ta-doped silver niobate are smaller than those of pure silver niobate, and this result may help us explain the remnant polarization of silver niobate. For silver niobate, there exists a remnant polarization of about 4 pC/cm^2 in the antiferroelectric hysteresis loop, and such remnant polarization decreases to be 2 pC/cm^2 after doping tantalum.⁴⁰ Previously, researchers thought that it is the ferrielectric Pmc_2_1 phase that causes the remnant polarization,^{40,42} but the hysteresis above 340 K (the phase transition temperature between Pmc_2_1 and Pbcm) also shows remnant polarization,⁴⁰ and, hence, there should be another reason.

As is known, ferroelectric materials will transform into the super paraelectric phase if the ferroelectric domains are small enough; at this time, the ferroelectric hysteresis loop will shrink to be a curve cross the origin. When it comes to the silver niobate

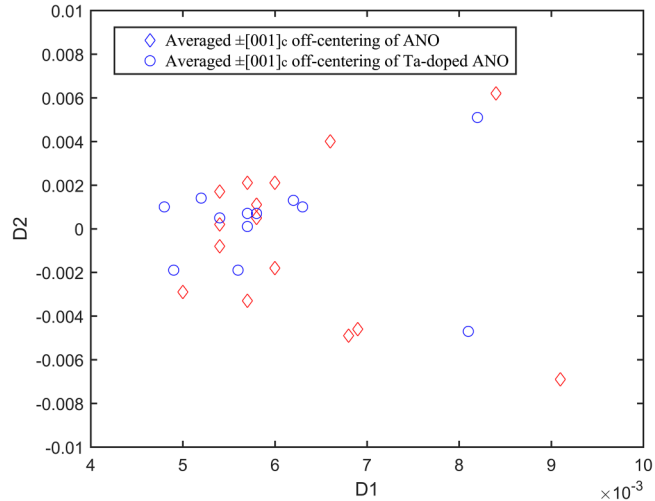


FIG. 5. Averaged $\pm[001]_c$ off-centering of silver niobate and Ta-doped silver niobate. Both D_1 and D_2 values of pure silver niobate are larger than those of Ta-doped silver niobate.

system, the vertical ordered displacement brings antiferroelectricity, and the weak ferroelectricity may result from the local $\pm[001]_c$ off-centering nanoregions, while the decreased remnant polarization after Ta doping can be well explained by the size decrease of the $\pm[001]_c$ off-centering regions. Recently, Tian *et al.* proposed that the remnant polarization may be a result of the polarization contributed by the field-induced ferroelectric phase,⁵⁵ which is consistent with our discussion above. In addition, the decrease of remnant polarization was beneficial for achieving higher energy storage density, which also partly explained the reason that tantalum doping increased the energy storage property of silver niobate.

IV. CONCLUSION

In conclusion, using a spherical-aberration-corrected STEM technique, and with the help of peak finding and Gaussian fitting, all the sites of cation columns in the HAADF images of silver niobate were quantitatively obtained. After calculations and analysis, it was found that B-site niobium ions also possessed off-centerings along the lateral $\pm[001]_c$ direction, which was perpendicular to the vertical $\pm[1-10]_c$ direction of antiferroelectric displacements. Contrary to the antiferroelectric displacements reported previously, such $\pm[001]_c$ off-centering was strongly localized. They formed a series of off-centering nanoregions similar to the polar nanoregions in relaxed ferroelectrics and may induce weak ferroelectricity. Such findings not only increase our understanding of antiferroelectric material presented by silver niobate in the microscopic view, but also may help explain some unsolved questions for long, such as the remnant polarization of silver niobate.

ACKNOWLEDGMENTS

This work was financially supported by the Chinese National Natural Science Foundation (Basic Science Center Project of NSFC

under Grant Nos. 51788104 and 11834009), the Basic and Applied Basic Research Major Program of Guangdong Province, China (Grant No. 2021B0301030003), and Jihua Laboratory (Project No. X210141TL210). This work made use of the resources of the National Center for Electron Microscopy in Beijing.

AUTHOR DECLARATIONS

Conflict of Interest

The authors have no conflicts to disclose.

DATA AVAILABILITY

The data that support the findings of this study are available from the corresponding authors upon reasonable request.

REFERENCES

- ¹N. X. Sun and G. Srinivasan, *Spin* **02**(3), 1240004 (2012).
- ²J. M. Liu, K. F. Wang, Y. Wang, Q. C. Li, and X. S. Gao, *Comput. Mater. Sci.* **30**(3–4), 389–396 (2004).
- ³Z. Zhou, X. Y. Zhang, T. F. Xie, T. X. Nan, Y. Gao, X. Yang, X. J. Wang, X. Y. He, P. S. Qiu, N. X. Sun, and D. Z. Sun, *Appl. Phys. Lett.* **104**, 012905 (2014).
- ⁴M. S. Mirshekarloo, N. Yakovlev, M. F. Wong, K. Yao, T. Sritharan, and C. S. Bhatia, *Appl. Phys. Lett.* **101**, 172905 (2012).
- ⁵J. P. Zhou, X. Z. Chen, L. Lv, C. Liu, and P. Liu, *Appl. Phys. A* **104**, 461–464 (2011).
- ⁶M. S. Mirshekarloo, K. Yao, and T. Sritharan, *Adv. Funct. Mater.* **22**(19), 4159–4164 (2012).
- ⁷W. P. Pan, Q. M. Zhang, A. Bhalla, and L. E. Cross, *J. Am. Ceram. Soc.* **72**(4), 571–578 (1989).
- ⁸M. S. Mirshekarloo, L. Zhang, K. Yao, and T. Sritharan, *Sens. Actuators A* **187**, 127–131 (2012).
- ⁹Z. Y. Liao, F. Xue, W. Sun, D. S. Song, Q. Q. Zhang, J. F. Li, L. Q. Chen, and J. Zhu, *Phys. Rev. B* **95**, 214101 (2017).
- ¹⁰S. S. N. Bharadwaja and S. B. Krupanidhi, *Mater. Sci. Eng. B* **78**, 1–10 (2000).
- ¹¹X. H. Hao, J. W. Zhai, and X. Yao, *J. Am. Ceram. Soc.* **92**(5), 1133–1135 (2009).
- ¹²J. Parui and S. B. Krupanidhi, *Appl. Phys. Lett.* **92**, 192901 (2008).
- ¹³M. Ye, Q. Sun, X. Q. Chen, Z. H. Jiang, F. P. Wang, and R. Whatmore, *J. Am. Ceram. Soc.* **94**(10), 3234–3236 (2011).
- ¹⁴M. S. Mirshekarloo, K. Yao, and T. Sritharan, *Appl. Phys. Lett.* **97**, 142902 (2010).
- ¹⁵B. M. Xu, P. Moses, N. G. Pai, and L. E. Cross, *Appl. Phys. Lett.* **72**, 593 (1998).
- ¹⁶H. L. Zhang, X. F. Chen, F. Cao, G. S. Wang, X. L. Dong, Z. Hu, and T. Du, *J. Am. Ceram. Soc.* **93**(12), 4015–4017 (2010).
- ¹⁷S. E. Young, J. Y. Zhang, W. Hong, and X. Tan, *J. Appl. Phys.* **113**, 054101 (2013).
- ¹⁸J. L. Li, Z. H. Shen, X. H. Chen, S. Yang, W. L. Zhou, M. W. Wang, L. H. Wang, Q. W. Kou, Y. C. Liu, Q. Li *et al.*, *Nat. Mater.* **19**(9), 999–1005 (2020).
- ¹⁹H. Pan, F. Li, Y. Liu, Q. H. Zhang, M. Wang, S. Lan, Y. P. Zheng, J. Ma, L. Gu, Y. Shen *et al.*, *Science* **365**(6453), 578–582 (2019).
- ²⁰M. Yashima, S. Matsuyama, R. Sano, M. Itoh, K. Tsuda, and D. S. Fu, *Chem. Mater.* **23**(7), 1643–1645 (2011).
- ²¹M. H. Francombe and B. Lewis, *Acta Crystallogr.* **11**(3), 175–178 (1958).
- ²²A. Kania, K. Roleder, and M. Łukaszewski, *Ferroelectrics* **52**, 265–269 (1984).
- ²³M. Verwerft, G. V. Tendeloo, J. V. Landuyt, W. Coene, and S. Amelinckx, *Phys. Status Solidi A* **109**(1), 67–78 (1988).
- ²⁴M. Verwerft, D. V. Dyck, V. A. M. Brabers, J. V. Landuyt, and S. Amelinckx, *Phys. Status Solidi A* **112**(2), 451–466 (1989).
- ²⁵A. Kania, *Ferroelectrics* **205**(1), 19–28 (1998).
- ²⁶J. Fábrý, Z. Zikmund, A. Kania, and V. Petříček, *Acta Crystallogr. C* **56**(8), 916–918 (2000).
- ²⁷A. Ratuszna, J. Pawluk, and A. Kania, *Phase Transitions* **76**(6), 611–620 (2003).
- ²⁸D. S. Fu, M. Endo, H. Taniguchi, T. Taniyama, and M. Itoh, *Appl. Phys. Lett.* **90**, 252907 (2007).
- ²⁹P. Sciau, A. Kania, B. Dkhil, E. Suard, and A. Ratuszna, *J. Phys. Condens. Matter* **16**, 2795–2810 (2004).
- ³⁰I. Levin, V. Krayzman, J. C. Woicik, J. Karapetrova, T. Proffen, M. G. Tucker, and I. M. Reaney, *Phys. Rev. B* **79**, 104113 (2009).
- ³¹I. Levin, J. C. Woicik, A. Llobet, M. G. Tucker, V. Krayzman, J. Pokorný, and I. M. Reaney, *Chem. Mater.* **22**, 4987–4995 (2010).
- ³²I. Grinberg and A. M. Rappe, *AIP Conf. Proc.* **677**, 130–138 (2003).
- ³³M. K. Niranjan and S. Asthana, *Solid State Commun.* **152**(17), 1707–1710 (2012).
- ³⁴H. Moriwake, C. A. J. Fisher, A. Kuwabara, and D. S. Fu, *Jpn. J. Appl. Phys.* **51**, 09LE02 (2012).
- ³⁵M. Yashima and S. Matsuyama, *J. Phys. Chem. C* **116**(47), 24902–24906 (2012).
- ³⁶Y. Tian, L. Jin, H. F. Zhang, Z. Xu, X. Y. Wei, E. D. Politova, S. Y. Stefanovich, N. V. Tarakina, I. Abrahams, and H. X. Yan, *J. Mater. Chem. A* **4**(44), 17279–17287 (2016).
- ³⁷L. Zhao, Q. Liu, S. J. Zhang, and J. F. Li, *J. Mater. Chem. C* **4**, 8380–8384 (2016).
- ³⁸Y. Tian, L. Jin, H. F. Zhang, Z. Xu, X. Y. Wei, G. Viola, I. Abrahams, and H. X. Yan, *J. Mater. Chem. A* **5**(33), 17525–17531 (2017).
- ³⁹L. Zhao, J. Gao, Q. Liu, S. J. Zhang, and J. F. Li, *ACS Appl. Mater. Interfaces* **10**, 819–826 (2018).
- ⁴⁰L. Zhao, Q. Liu, J. Gao, S. J. Zhang, and J. F. Li, *Adv. Mater.* **29**(31), 1701824 (2017).
- ⁴¹J. Gao, Y. Zhang, L. Zhao, K.-Y. Lee, Q. Liu, A. Studer, M. Hinterstein, S. Zhang, and J.-F. Li, *J. Mater. Chem. A* **7**, 2225–2232 (2019).
- ⁴²J. Gao, Q. Liu, J. F. Dong, X. Wang, S. J. Zhang, and J. F. Li, *ACS Appl. Mater. Interfaces* **12**(5), 6097–6104 (2020).
- ⁴³S. Li, H. C. Nie, G. S. Wang, C. H. Xu, N. T. Liu, M. X. Zhou, F. Cao, and X. L. Dong, *J. Mater. Chem. C* **7**(6), 1551–1560 (2019).
- ⁴⁴Z. N. Yan, D. Zhang, X. F. Zhou, H. Qi, H. Luo, K. C. Zhou, I. Abrahams, and H. X. Yan, *J. Mater. Chem. A* **7**(17), 10702–10711 (2019).
- ⁴⁵K. Han, N. N. Luo, S. F. Mao, F. P. Zhuo, L. J. Liu, B. L. Peng, X. Y. Chen, C. Z. Hu, H. F. Zhou, and Y. Z. Wei, *J. Mater. Chem. A* **7**(46), 26293–26301 (2019).
- ⁴⁶Z. L. Lu, W. C. Bao, G. Wang, S. K. Sun, L. H. Li, J. L. Li, H. J. Yang, H. F. Ji, A. Feteira, F. F. Xu *et al.*, *Nano Energy* **79**, 105423 (2021).
- ⁴⁷T. Y. Li, W. J. Cao, P. F. Chen, J. S. Wang, and C. C. Wang, *J. Mater. Sci.* **56**, 13499–13508 (2021).
- ⁴⁸Y. L. Zhang, X. B. Li, J. M. Song, S. W. Zhang, J. Wang, X. H. Dai, B. T. Liu, G. Y. Dong, and L. Zhao, *J. Materiomics* **7**(6), 1294–1300 (2021).
- ⁴⁹G. Li, H. Liu, L. Zhao, J. Gao, J. F. Li, R. Yu, and J. Zhu, *Appl. Phys. Lett.* **113**, 242901 (2018).
- ⁵⁰G. Li, H. Liu, L. Zhao, J. Gao, S. Y. Liang, J. F. Li, and J. Zhu, *J. Appl. Phys.* **125**, 204103 (2019).
- ⁵¹T. Ma, Z. M. Fan, B. Xu, T.-H. Kim, P. Lu, L. Bellaiche, M. J. Kramer, X. L. Tan, and L. Zhou, *Phys. Rev. Lett.* **123**, 217602 (2019).
- ⁵²Z. Q. Fu, X. F. Chen, Z. Q. Li, T. F. Hu, L. L. Zhang, P. Lu, S. J. Zhang, G. S. Wang, X. L. Dong, and F. F. Xu, *Nat. Commun.* **11**, 3809 (2020).
- ⁵³C. Ophus, J. Ciston, and C. T. Nelson, *Ultramicroscopy* **162**, 1–9 (2016).
- ⁵⁴V. Krayzman and I. Levin, *J. Phys. Condens. Matter* **22**, 404201 (2010).
- ⁵⁵Y. Tian, J. Li, Q. Y. Hu, L. Jin, K. Yu, J. L. Li, E. D. Politova, S. Y. Stefanovich, Z. Xu, and X. Y. Wei, *J. Mater. Chem. C* **7**(4), 1028–1034 (2019).